ISSN 1063-7834, Physics of the Solid State, 2018, Vol. 60, No. 6, pp. 1163–1167. © Pleiades Publishing, Ltd., 2018.
Original Russian Text © D.S. Kuchin, P.V. Lega, A.P. Orlov, A.V. Frolov, A.V. Irzhak, A.M. Zhikharev, A.P. Kamantsev, V.V. Koledov, A.V. Shelyakov, V.G. Shavrov, 2018, published in Fizika Tverdogo Tela, 2018, Vol. 60, No. 6, pp. 1152–1156.

## MECHANICAL PROPERTIES, PHYSICS OF STRENGTH, AND PLASTICITY

# High-Speed Composite Microactuator Based on $Ti_2NiCu$ Alloy with Shape Memory Effect

**D. S. Kuchin[a], P. V. Lega[a, *], A. P. Orlov[a], A. V. Frolov[a], A. V. Irzhak[b, c], A. M. Zhikharev[a], A. P. Kamantsev[a], V. V. Koledov[a, e], A. V. Shelyakov[d], and V. G. Shavrov[a, **]**

[a] *Kotelnikov Institute of Radio Engineering and Electronics, Russian Academy of Sciences, Moscow, 125009 Russia*
[b] *National University of Science and Technology "MISiS," Moscow, 119049 Russia*
[c] *Institute of Technological Problems of Microelectronics and Ultrapure Materials, Russian Academy of Sciences, Chernogolovka, Moscow oblast, 142432 Russia*
[d] *National Research Nuclear University "MEPhI," Moscow, 115409 Russia*
[e] *Institute for Nanotechnology in Micrtoelectronics, Russian Academy of Science, Moscow, 115487 Russia*
**e-mail: lega_peter@list.ru*
***e-mail: shavrov@cplire.ru*
Received December 11, 2017

**Abstract**—Samples of microactuators are made of a bimorph composite of $Ti_2NiCu$ alloy with a thermoelastic martensitic transition and the shape memory effect, and their response rate is investigated. The active layer of the composite actuator is a layer of the rapidly quenched $Ti_2NiCu$ alloy, pseudoplastically prestretched, and an amorphous layer of the same alloy is used as an elastic layer. Typical sizes of the microactuator are $30 \times 2 \times 2$ μm. The controlled amplitude of the displacement of the microactuator tip is approximately 1 μm. The response rate of the microactuator was investigated by scanning electron microscopy. Activation of the microactuator was achieved by heating when electric pulses were passed through it. Full activation of the microactuator at frequencies up to 1 kHz was demonstrated; partial activation was observed at frequencies up to 8 kHz. The possibility of operating the device in a self-oscillating mode at frequencies of the order of 100 kHz is demonstrated.

**DOI:** 10.1134/S1063783418060173

## 1. INTRODUCTION

The effect of shape memory is the returning of matter to the initial spatial configuration during heating, which is observed in some materials after preliminary deformation, in particular, in intermetallic alloys after deformation in the thermoelastic martensitic phase transition from the high-symmetric high-temperature (austenite) phase to the low-symmetric low-temperature (martensite) phase, which takes place during cooling. Alloys with the shape memory effect have a set of excellent properties, including high strength of the material (mechanical stress can reach hundreds of megapascals) [1], the ability to return large deformations (up to 10%) and generate considerable force during heating [2] or under the action of a magnetic field [3–6], superelasticity (up to 14%), high damping ability [7], good corrosion resistance [8], and biocompatibility [9]. At present, a large number of intermetallic alloys with the shape memory effect are known, for example, NiTi, $Ti_2NiCu$, CuAlNi, CuZnAl, $Ni_2MnGa$, and others. They have found wide application in various fields of technology, in particular, medicine, instrument engineering, space engineering, etc. [10, 11]. In the case where the shape memory effect is manifested under the thermal action on the material, it is necessary to organize periodic supply and heat removal for the cyclic operation of devices including such materials. Controlling the device through heating and cooling may seem like a nontechnological solution, as the heat processes, especially when cooling, are quite inert. However, as the size of the device decreases, the characteristic times of the thermal processes decrease quadratically. This opens the prospect of creating high-speed miniature devices based on alloys with the shape memory effect. The goal of this work is the creation and experimental study of the response rate of miniature actuators based on $Ti_2NiCu$ alloy with the shape memory effect when activated by pulses of electric current.

## 2. SAMPLES AND METHODS

A bimetallic composite is used in this work for the implementation of multiple reversible bending deformations in thin samples of alloys with the shape memory effect. For the manufacture of the actuator, we

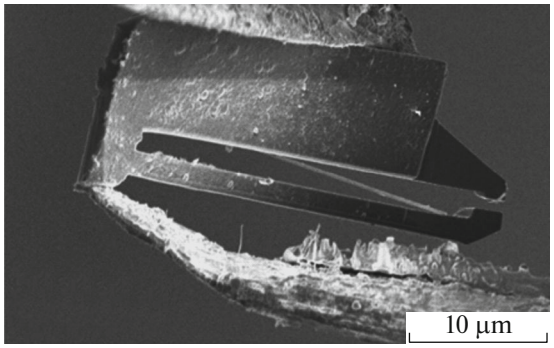


**Fig. 1.** Composite actuator in the open state. The needles of manipulators are used as conductors of electric current.

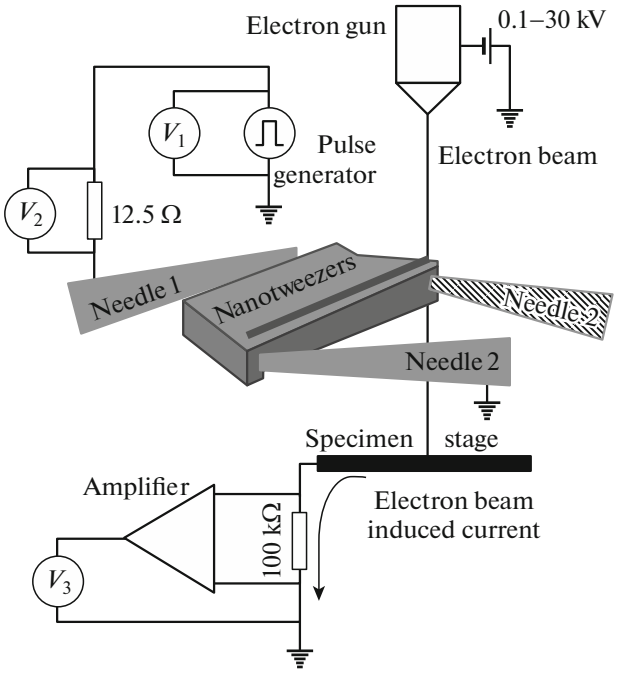


**Fig. 2.** Schematic diagram of the experimental setup.

used rapidly quenched ribbons of $Ti_2NiCu$ alloy with the shape memory effect, obtained by ultrafast melt quenching on a rotating copper disk [12]. In the crystalline state, the alloy exhibits a thermoelastic martensitic transformation of the first kind from the austenitic phase B2 with a cubic lattice to the martensitic phase B19 with an orthorhombic lattice [13]. The temperatures of the beginning and the end of the forward and reverse martensitic transitions are $M_s$ = 60°C, $M_f$ = 52°C, $A_s$ = 55°C, and $A_f$ = 64°C, respectively.

To prepare microactuators, the ribbons were preliminarily subjected to pseudoplastic tensile deformation: they were heated to a temperature above $A_f$ and then cooled to a temperature below $M_f$ under a tensile load of 3–10 N. Then, the edges of the ribbon were soldered by electrochemical etching to a thickness of the order of 2–3 μm. At the second stage, the body of the actuator was formed on the edge of the ribbon using a focused ion beam (FIB) assembly. The next stage was the application of an elastic layer by etching an auxiliary hole in the ribbon using a focused ion beam. As a result, the sprayed alloy was deposited on the body of the actuator and amorphized, thus forming an elastic layer on the surface of the prestretched $Ti_2NiCu$ layer. All stages of manufacturing of the microactuator were carried out at a temperature below $M_f$ of the austenite–martensite transition. The procedure for forming a composite actuator with an elastic amorphous layer is described in more detail in [14, 15].

Upon heating above the martensite–austenite phase transition temperature ($A_f$), the active layer of the actuator decreases because of the presence of a pseudoplastic strain in it, while the length of the elastic layer does not change, which leads to a bending of the actuator, that is, to its actuation. When cooling below the temperature of the austenite-martensite transition ($M_f$), the actuator is straightened by the elastic layer [16].

The heating of the actuator was carried out by passing an electric current through its body. To implement this circuit in a vacuum chamber of a scanning electron microscope (SEM), the sample was attached to a tungsten needle of the Kleindiek micromanipulator. Another tungsten needle attached to the second manipulator was brought to the sample to form a closed electrical circuit (Fig. 1). The simulation of current flow and consequence heat release as well as heat propagation was done to prevent the overheating of the system and to estimate the time of operation of the actuator. The total electrical resistance of the circuit consisting of the sample, the needles of the manipulators, and the supply wires was in the range of 20–100 Ω and was determined mainly by the quality of the contact between the actuator body and the needle of the second micromanipulator. The actuation current of the actuator was within the range of 4–11 mA. To investigate the actuation speed of the actuator, a CrossbeamNeon 40 EsB SEM was used. A schematic diagram of the experimental setup is shown in Fig. 2.

## 3. RESULTS AND DISCUSSION

A study of the response rate of the microactuator at low frequencies was performed visually on the SEM display. To reduce the sweep time of the frame, the scanning area was limited to a region of approximately 1 $\mu m^2$, immediately near the tip (Fig. 3). Thus, the operation of the device (clamp-open cycle) could be detected reliably with a duration of the control electric pulse not shorter than 5 ms. A further decrease in the duration of the current pulse led to the fact that the sweep time of the SEM frame even in such a small region was much higher than the characteristic actuation time of the microactuator. In the case of visual observation, the actuation of the actuator occurs

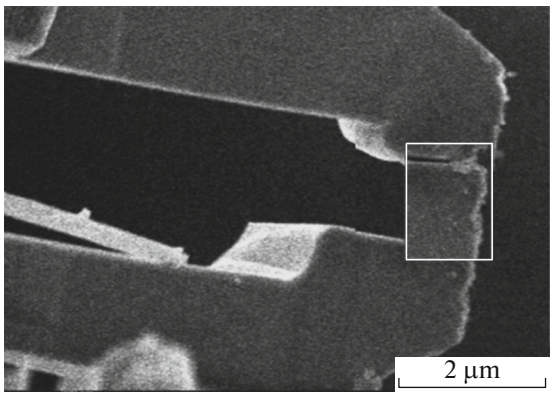


**Fig. 3.** Composite actuator. The scanning area of the SEM for visual monitoring of actuation of the actuator is marked with a white frame.

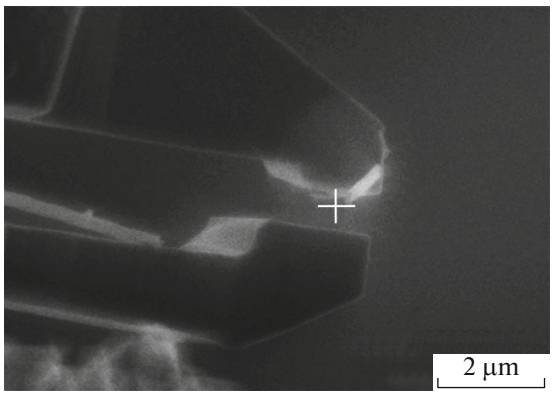


**Fig. 4.** Composite actuator. A white cross marks the place of focusing of the SEM electron beam.

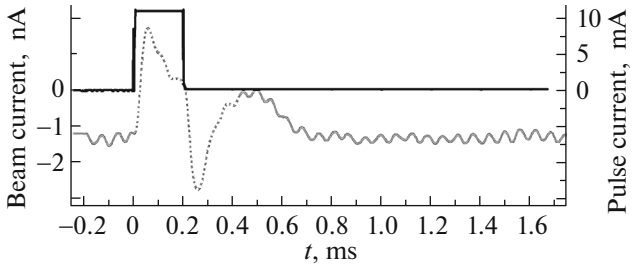


**Fig. 5.** Time dependence of actuation of the actuator and control voltage for a pulse length of 200 μs. The upper curve indicates the control voltage; the lower curve is the signal from the SEM electron beam.

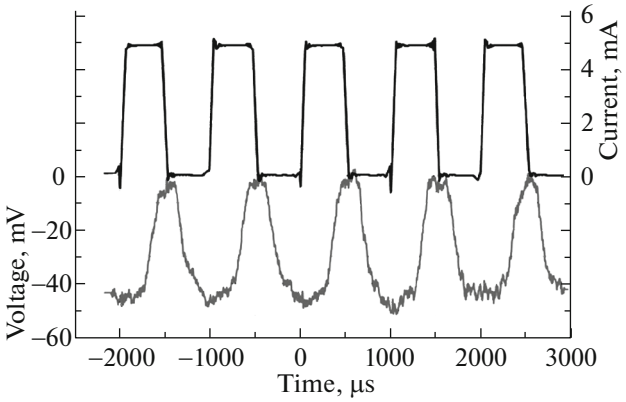


**Fig. 6.** Time dependence of actuation of the actuator and control voltage for a pulse length of 500 μs. The upper curve indicates the control voltage; the lower curve is the signal from the SEM electron beam.

almost instantaneously when an electric current pulse is applied.

To conduct further research at higher frequencies (shorter electrical pulses), the measurement procedure was changed. A narrow electron beam with a diameter of several nanometers was focused on the SEM object table at a point in the immediate vicinity of the actuator tip so that the electron beam was interrupted at the actuation of the actuator (Fig. 4). The current of the electron beam in the course of the measurements was 1 nA. The SEM object table is grounded through a load resistor of 100 kΩ, to which a digital oscilloscope was connected. When the actuator interrupted the electron beam, the voltage on the load resistor of the object table became zero, which made it possible to record the fact of the operation of the micromechanical device.

A number of dependences were obtained in the measurements, both for single pulses and for periodic pulse sequences. The pulse duration varied from 200 ms to 50 μs, which corresponds to frequencies in the range from 5 Hz to 20 kHz. Figure 5 demonstrates the oscillogram of the time dependence of the current pulses (the upper line) and the voltage on the load resistor (bottom line) for pulses of 200 μs in duration. The dashed line on the bottom line of the oscillogram shows the part of the signal, corresponding to the noise that occurs in the make-and-break of the electrical circuit. This noise was measured and then subtracted from the signal during processing. An example of the processed oscillogram is shown in Fig. 6; it corresponds to a pulse duration of 500 μs and a pulse repetition rate of 1 kHz, with a noticeable delay time between the activation pulse and actuation of the actuator.

It is accepted that the actuator with the shape memory, presented in [17], demonstrated the best response rate, according to the analysis of publications all over the world. The cited paper describes the work of a composite actuator based on Ti–Ni microwires with a frequency of controlled deformations of 35 Hz. In this regard, the actuator presented in this work is record-setting for the response rate.

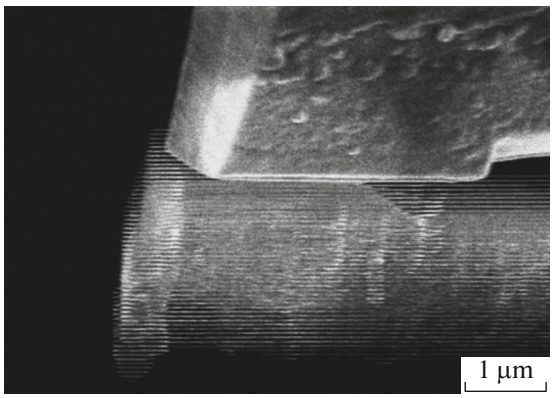


**Fig. 7.** Vibration of the actuator at high frequencies of control voltage. The sweep time of the SEM frame is much shorter than the oscillation period.

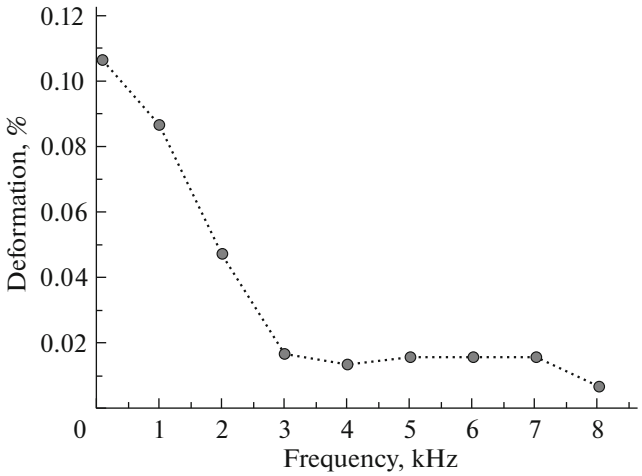


**Fig. 8.** Dependence of the relative strain on the control voltage frequency ranged 1–8 kHz.

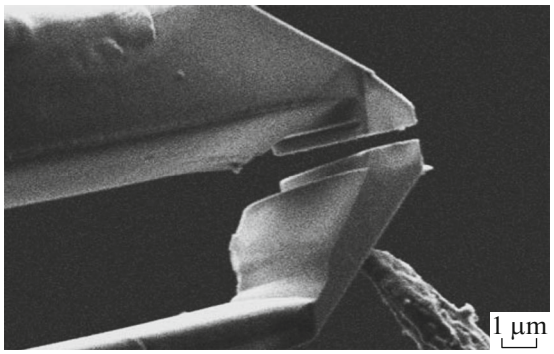


**Fig. 9.** Position of the micromanipulator needle for observing self-oscillations.

Detection of oscillations at frequencies above 1 kHz becomes difficult due to the increase in noise. However, the oscillations of the actuator can be observed visually at frequencies up to 20 kHz (Fig. 7).

As the frequency of the control voltage increases, the amplitude of the deviation of the microactuator decreases noticeably. Having estimated the amplitude of oscillations λ from the vibration of the actuator visually observed in the SEM, we can calculate the values of the relative deformation of the alloy with the shape memory effect, namely,

$$\varepsilon = \frac{h\lambda}{L^2}, \quad (1)$$

where $h$ is the thickness of the actuator, and $L$ is its length. The obtained data for the frequency of the control voltage from 1 to 8 kHz are shown in Fig. 8. Despite the sharp drop in the amplitude of the oscillations in the range from 1 to 3 kHz, the actuator remains partially operable at frequencies up to 8 kHz.

Furthermore, a study was made of the operation of the actuator in the self-oscillating mode. In these measurements, the needle of the second manipulator moved to the position shown in Fig. 2 by a dashed contour. The SEM image of the relative positioning of the actuator and the manipulator needle is given in Fig. 9. When the electric current passes, the actuator is heated and actuated. Then, the electrical circuit breaks as a result of its bending deformation. Then the cooling takes place, and the actuator returns to its original position, which leads to the closure of the electrical circuit. Thus, the actuator reaches the self-oscillating mode. It was demonstrated that in the self-oscillating mode, the actuation frequency of the actuator could exceed 100 kHz (Fig. 10).

## 4. CONCLUSIONS

The following results are obtained:

1. Samples of microactuators based on amorphous-crystalline composites of $Ti_2NiCu$ alloy with dimensions of 30 × 2 × 2 μm are prepared, having controlled deformation with an amplitude of 1 μm. The minimum response time of the microactuator is 700 μs when activated by pulses of electric current.

2. The maximum frequency of actuation of the microactuator under periodic excitation by current pulses is 1 kHz, with a partial activation of the microactuator observed at a frequency of 20 kHz.

3. In the self-oscillating mode, the response frequency of the microactuator can exceed 100 kHz.

Thus, the paper demonstrates a micromechanical device recordbreaking in response rate, based on an alloy with a shape memory effect. In our opinion, such devices can find application in the technology of micro- and nanoelectromechanical systems for the creation of actuators and robotic devices, in lab-on-a-chip technology, microbiology, for biological (DNA,

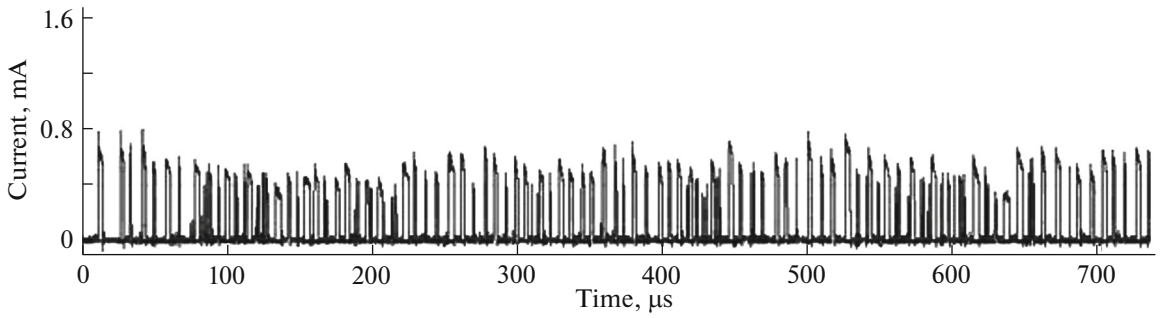


**Fig. 10.** Time dependence of the current flow through the actuator when a constant voltage is applied. The frequency of the current pulses caused by self-oscillations of the microactuator is more than 100 kHz.

insulin sensitivity, etc.) and nonbiological (carbon nanotubes, graphene layers, whiskers) micro- and nanoobjects. Despite the achieved relatively high response frequencies, these values are far from the frequencies of mechanical resonance, which according to the authors' estimates by the model of a physical pendulum are of the order of 10 MHz. Once the resonant frequencies correlated with the rate of thermal processes are achieved, it becomes possible to produce a device with an even higher response rate and with a larger relative strain. For this purpose, apparently, it is necessary to decrease the dimensions of the microactuator to 1 μm or less.

## ACKNOWLEDGMENTS

The work was supported by the Russian Science Foundation, project no. 17-19-01748. The simulation was supported by the Russian Foundation for Basic Research (project no. 18-37-00466).

## REFERENCES

1. H. Sehitoglu, I. Karaman, R. Anderson, X. Zhang, K. Gall, H. J. Maier, and Y. I. Chumlyakov, Acta Mater. **49**, 747 (2001).
2. J. Shaw and S. Kyriakides, J. Mech. Phys. Solids **43**, 1243 (1995).
3. A. D. Bozhko, V. D. Buchel'nikov, A. N. Vasil'ev, I. E. Dikshtein, S. M. Seletskii, V. V. Khavailo, and V. G. Shavrov, JETP Lett. **67**, 227 (1998).
4. V. Buchelnikov, I. Dikshtein, R. Grechishkin, T. Khudoverdyan, V. Koledov, Y. Kuzavko, I. Nazarkin, V. Shavrov, and T. Takagi, J. Magn. Magn. Mater. **272–276**, 2025 (2004).
5. N. I. Kourov, A. V. Korolev, V. G. Pushin, V. V. Koledov, V. G. Shavrov, and V. V. Khovailo, Phys. Met. Metallogr. **99**, 376 (2005).
6. V. G. Pushin, N. I. Kourov, A. V. Korolev, V. A. Kazantsev, L. I. Yurchenko, V. V. Koledov, V. G. Shavrov, and V. V. Khovailo, Phys. Met. Metallogr. **99**, 401 (2005).
7. S. Saadat, J. Salichs, and M. Noori, Smart Mater. Struct. **11**, 218 (2002).
8. D. Wever, A. Veldhuizen, J. de Vries, H. J. Busscher, D. R. A. Uges, and J. R. van Horn, Biomaterials **19**, 761 (1998).
9. L. Ponsonnet, D. Treheux, and M. Lissac, Int. J. Appl. Electromagn. Mech. **23**, 147 (2006).
10. K. Otsuka and X. Ren, Prog. Mater. Sci. **50**, 511 (2005).
11. J. M. Jani, M. Leary, A. Subic, and M. A. Gibson, Mater. Des. **56**, 1078 (2014).
12. *Shape Memory Alloys: Fundamentals, Modeling and Industrial Applications*, Ed. by A. V. Shelyakov, N. M. Matveeva, S. G. Larin, F. Trochu, V. Brailovski, and A. Galibois (Canad. Inst. Mining, Metall. Pet., Quebec City, Canada, 1999), p. 295.
13. P. L. Potapov, S. E. Kulkova, A. V. Shelyakov, K. Okutsu, S. Miyazaki, and D. Schryvers, J. Phys. IV **112**, 727 (2003).
14. P. Lega, V. Koledov, A. Orlov, D. Kuchin, A. Frolov, V. Shavrov, A. Martynova, A. Irzhak, A. Shelyakov, V. Sampath, V. Khovaylo, and P. Ari-Gur, Adv. Eng. Mater. **19**, 1700154 (2017).
15. A. M. Zhikharev, A. V. Irzhak, M. Y. Beresin, P. V. Lega, V. V. Koledov, N. N. Kasyanov, and G. S. Martynov, J. Phys.: Conf. Ser. **741**, 012206 (2016).
16. A. V. Irzhak, P. V. Lega, A. M. Zhikharev, V. V. Koledov, A. P. Orlov, D. S. Kuchin, N. Y. Tabachkova, V. A. Dikan, A. V. Shelyakov, M. Y. Beresin, V. G. Pushin, S. V. von Gratowski, V. Y. Pokrovskiy, S. G. Zybtsev, and V. G. Shavrov, Dokl. Phys. **62**, 5 (2017).
17. S. H. Song, J-Y. Lee, H. Rodrigue, I-S. Choi, Y. J. Kang, and S. H. Ahn, Sci. Rep. **6**, 21118 (2016).

*Translated by O. Zhukova*